Model Based Multiscale Detection and Reconstruction of 3D Vessels

Karl Krissian, Grégoire Malandain, Nicholas Ayache

INSTITUT NATIONAL DE RECHERCHE EN INFORMATIQUE ET EN AUTOMATIQUE

Model Based Multiscale Detection and Reconstruction of 3D Vessels

Karl Krissian — Grégoire Malandain — Nicholas Ayache

N° 3442

June 1998

THÈME 3

ISSN 0249-6399

INRIA
SOPHIA ANTIPOLIS

Model Based Multiscale Detection and Reconstruction of 3D Vessels

Karl Krissian , Grégoire Malandain , Nicholas Ayache

Thème 3 — Interaction homme-machine,
images, données, connaissances
Projet Epidaure

Rapport de recherche n° 3442 — June 1998 — 26 pages

Abstract: The segmentation of 3D brain vessels is an important issue for physicians in order to operate an aneurysm. We introduce new vessel models for selecting a subset of interesting points near the vessel center. We also present a new approach to segment and reconstruct 3D brain vessels. The response at one scale is obtained by integrating along a circle the first derivative of the intensity in the radial direction. We also use a vessel model to choose a good parameter for a γ-normalization of the response obtained at each scale. Once the parameter γ is fixed, we find the relation between a vessel radius and the scale at which it is detected. From the multiscale response, we create a smoothed skeleton of the vessels and we reconstruct the vessels from their centerlines and their radii. The method has been tested on a large variety of 3D images of cerebral vessels, with excellent results. Vessels of various size and contrast are detected with remarkable robustness, even when they are close or tangent to another vessel, and most junctions are preserved. Results are obtained in a few minutes on a Dec-Alpha workstation, for a 128^3 image. This work was done in collaboration with General Electric Medical Systems Europe (GEMSE).

Key-words: filtering, vessel detection, multiscale analysis, segmentation.

Unité de recherche INRIA Sophia Antipolis
2004, route des Lucioles, B.P. 93, 06902 Sophia Antipolis Cedex (France)
Téléphone : 04 92 38 77 77 - International : +33 4 92 38 77 77 —Fax : 04 92 38 77 65 - International : +33 4 92 38 77 65

Détection et Reconstruction multi-échelle de vaisseaux dans des images tridimensionnelles

Résumé : La segmentation de vaisseaux dans des images cérébrales tridimensionnelles peut fournir une information précieuse au médecin lors de l'opération d'un anévrisme. Nous introduisons de nouveaux modèles de vaisseaux, dont l'étude permet de sélectionner un ensemble de points situés au voisinage des axes des vaisseaux. Nous introduisons aussi une nouvelle approche permettant de segmenter et de reconstruire les vaisseaux dans des images tridimensionnelles. La réponse à une échelle donnée est obtenue par intégration de la dérivée première de l'intensité dans la direction radiale le long d'un cercle situé dans le plan d'une section du vaisseau. L'utilisation d'un modèle permet aussi de choisir un bon paramètre γ de normalisation. Une fois le paramètre γ fixé, nous en déduisons la relation entre le rayon d'un vaisseau et l'échelle à laquelle il est détecté. La réponse multi-échelle nous permet alors d'obtenir un squelette des vaisseaux et de reconstruire le réseau vasculaire à partir des axes et des rayons associés. La méthode a été testée sur plusieurs images tridimensionnelles de vaisseaux du cerveau avec de très bons résultats. Les vaisseaux de différentes tailles et de différentes intensités sont détectés avec une robustesse remarquable, même lorsqu'ils sont proches ou tangents. La plupart des jonctions sont préservées. Le temps de calcul est de quelques minutes sur une station DEC-Alpha, pour une image 128^3. Ce travail a été réalisé en collaboration avec General Electric Medical System Europe (GEMSE).

Mots-clés : filtrage, détection de vaisseaux, traitement multi-échelle, segmentation.

Contents

1 Introduction

The purpose of this work is to detect the structure of the vessels in 3D angiographies of the brain in order to help the interpretation of the vessels network, especially in the vicinity of aneurysms. This report is an extension of previous work on 3D multiscale vessel detection [KMAV98a, KMAV98b]. Few works were done in the detection of 3D complex vessels network. Our work is based on previous works already done by Koller et al [KGSD95], Lorenz et al [LCBF97], Pizer et al [PEFM98], Fritsch et al [FPME94, FEPM95], Lindeberg [Lin96, Lin94]. It is also closed to the work of [SNAK97]. We introduce a multi-scale method based on a new response function which measures the contours of a vessel around the centerlines. Moreover, a cylindrical model of vessel allows us to find good parameters for our method. We will successively present the acquisition process, related approaches, our method, results and conclusion.

2 Image Acquisition

The images were produced by GEMSE. They are obtained by 3D reconstruction of the vessels from 2D X-ray substracted angiographies. Details of the reconstruction scheme can be found in [Pay96]. Compared to the other 3D acquisition modalities which are Magnetic Resonance Angiography and Scanner Angiography, this 3D reconstruction gives a high isotropic resolution over the whole reconstructed volume. Nevertheless, it requires a good opacification of the vascular network obtained with an intra-arterial injection. Some MIPs of 3D images centered on an aneurysm are shown in Fig. 1. The images we are dealing with contain different artefacts:

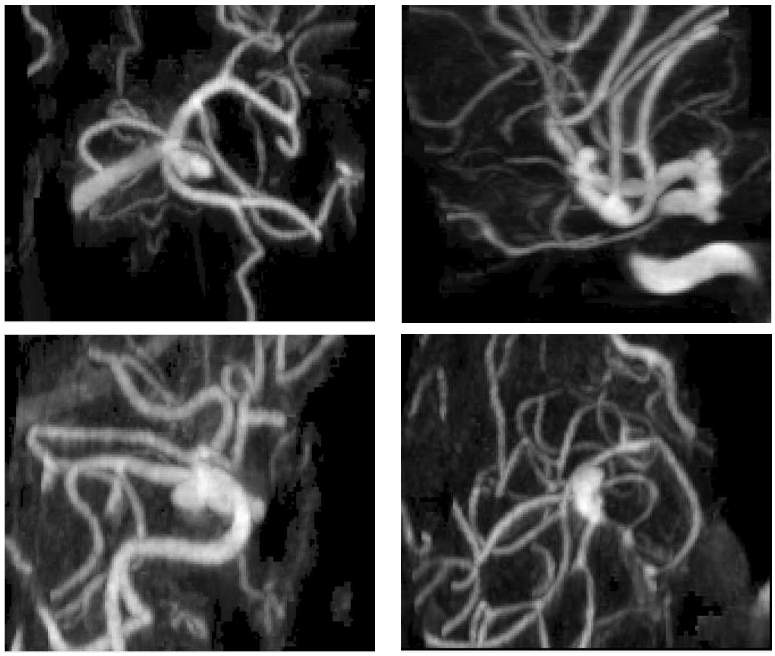

Figure 1: Maximum Intensity Projection of 4 different 3D images (images are $128 \times 128 \times 128$).

noise, partial volume effect, consequences of the patient motion between different acquisitions and 3D reconstruction artefacts which lead to a non-homogeneity of the intensity of the vessels

for different sizes of the vessel (Fig. 2 shows three isosurfaces of the initial image; small vessels are only visible with a low threshold).

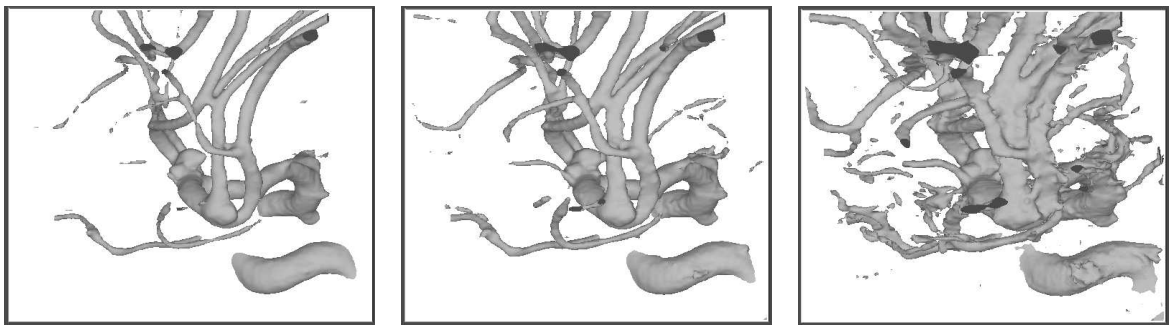

threshold 1138 threshold 871 threshold 500

Figure 2: Isosurfaces of the top right image of Fig. 1 with different thresholds.

3 Multiscale extraction of vessels

The general approach of multiscale methods is to choose a range of scales and to compute a response for each scale from the initial image. All the responses are then combined to get a single multiscale response which contains the sought after features. The foundations of the scale-space theory can be found in [Lin94]. More formally, for a fixed scale s, we calculate a response image for that scale, $R_s(I)$, where I is the initial image. Then we calculate the multiscale response for the image $R_{multi}(I)$ which for each point $x \in I$ gives the maximum of the responses over a range $[s_l, s_h]$ of scales:

$$R_{multi}(x) \;=\; \max_s \{R_s(x), s \in [s_l, s_h]\}\,. \tag{1}$$

This response $R_{multi}(x)$ can be interpreted as an indicator that the point x belongs to the center line of a vessel, and $R_s(x)$ can be interpreted as an indicator that the point x belongs to the center line of a vessel with radius s.
The main problem is to choose the response function at a single scale. Two different approaches have been proposed, the first one is based on first derivatives of the intensity [KGSD95] and the second one is based on second derivatives of the intensity [LCBF97, SNAK97]. In both cases, the response is chosen in order to discriminate edges and sheet-like structures from vessel-like structures. In [KGSD95], $R_s(I)$ is taken as the minimum of the absolute value of the first

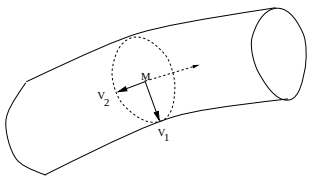

derivative at x_i in the direction of $\mathbf{x}\vec{\mathbf{x}}_\mathbf{i}$ for the 4 points ($x_i \in \{x \pm s\vec{\mathbf{v}}_1, x \pm s\vec{\mathbf{v}}_2\}$).

$$R_s(x) = \min\left\{\left|\nabla I_s(x + s\vec{\mathbf{v}}).\vec{\mathbf{v}}\right|, \vec{\mathbf{v}} \in \{\pm\vec{\mathbf{v}}_1, \pm\vec{\mathbf{v}}_2\}\right\} \tag{2}$$

where $I_s = I * G_s$ is the image convolved with a Gaussian, G_s, with standard deviation s, and $(\vec{\mathbf{v}}_1, \vec{\mathbf{v}}_2)$ is a basis of unitary vectors in the plane orthogonal to the vessel axis. The vectors $\vec{\mathbf{v}}_1$

and $\vec{\mathbf{v}}_2$ are obtained from the eigenvectors of the Hessian matrix, H^*, of the image at a given scale $s = \sigma$: $H^*(x) = H_\sigma(x) = H(I * G_\sigma)(x)$. We denote the eigenvalues of H^* as $\lambda_1, \lambda_2, \lambda_3$ and the associated unitary eigenvectors as $\vec{\mathbf{v}}_1, \vec{\mathbf{v}}_2, \vec{\mathbf{v}}_3$; with $\mid \lambda_1 \mid \geq \mid \lambda_2 \mid \geq \mid \lambda_3 \mid$.
In [LCBF97], the authors distinguish four cases depending on the structure (line or plane) and on its intensity (bright or dark). In the case of a bright structure with a dark background,

$$\textbf{line} \quad \lambda_1, \lambda_2 < 0; \quad |\lambda_1|, |\lambda_2| \gg |\lambda_3|, \quad \textbf{plane} \quad \lambda_1 < 0; \quad |\lambda_1| \gg |\lambda_2|, |\lambda_3|. \tag{3}$$

For vessels, the eigenvector $\vec{\mathbf{v}}_3$ associated with λ_3 will give the direction of the axis whereas $\vec{\mathbf{v}}_1$ and $\vec{\mathbf{v}}_2$ will give a basis in the plane orthogonal to the axis. This criterion, based on an interpretation of the Taylor expansion of 2nd order of the intensity function, will be studied more rigorously below on different vessel models.

4 Our method

Our approach is an extension of [KGSD95] dedicated to three dimensional images. It can be split into three steps. We first compute the multiscale response $R_{multi}(I)$ from responses at a discrete set of scales, we then extract the local extrema R^e_{multi} in $R_{multi}(I)$, and finally we create a skeleton of R^e_{multi} and visualize the results. Vessels are also reconstructed using both the centerlines and the size information. In the first step, we use a model of the vessels both for interpreting the eigenvalues and the eigenvectors of the Hessian matrix and for choosing a good normalization parameter.

Computation of the *single scale response* requires different steps. First, a number of points are pre-selected using the eigenvalues of the Hessian matrix. These points must be near a vessel axis. Then, for each pre-selected point, the response is computed at the current scale. The response function, derived from equation (2), uses every point of a circle, not just the four points. Finally, this response is normalized in order to give a multiscale scale response that combines interesting features of each single scale response. These steps are detailed in the following paragraphs.

4.1 Choice of an initial model

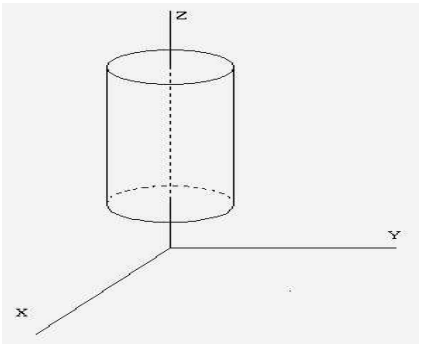

Figure 3: Initial model of a vessel.

The first vessel model that we introduce is cylindrical where (Oz) is the vessel axis and the vessel section is a Gaussian blob:

$$I_0(x, y, z) = C\, G_{\sigma_0}(x, y) = \frac{C}{2\pi {\sigma_0}^2} e^{-\frac{x^2+y^2}{2{\sigma_0}^2}}. \tag{4}$$

where C is a function of σ_0 and $\frac{C}{2\pi{\sigma_0}^2}$ represents the intensity at the center of the vessel (Fig. 3). C depends on the size of the vessel, this dependence is due to partial volume effect that decreases the small vessels intensity.

The model properties are:

- the frontier of the vessel is considered to be at the points where the first derivative in the gradient direction is maximum, i.e., for the points which verify $x^2 + y^2 = {\sigma_0}^2$, thus the vessel radius is σ_0.
- if the model is convolved with a Gaussian kernel of standard deviation s, the resulting image is another vessel which matches our model but with a different radius. This result can be directly deduced from the semi-group property.

In order to better take into account the reality of the vessels, we will study two variations of this model. The first one is a toric circular vessel which allows us to introduce a curvature of the vessel. The second one is a cylindrical vessel with an elliptical cross-section which introduces a variation in the circular shape of the vessel.

4.2 Pre-selection of candidates using eigenvalues of the Hessian matrix

In order to compute the response at one scale $R_s(I_0)$, we need a pre-selection of the points that are near the axis of a vessel, and also a good estimation of the vectors $\vec{\mathbf{v}}_1$ and $\vec{\mathbf{v}}_2$ that give an orthogonal basis in the plane of a section. In [LCBF97], the authors noticed (equation (3)) that a first criterion to detect line-like structures can be defined using the eigenvalues of the Hessian matrix. A formal derivation of our model allows us to check this criterion.

4.2.1 Cylindrical circular model

The Hessian matrix can be expressed as $H = \frac{I_0}{{\sigma_0}^4} H_0$ where

$$H_0 = \begin{bmatrix} x^2 - {\sigma_0}^2 & xy & 0 \\ xy & y^2 - {\sigma_0}^2 & 0 \\ 0 & 0 & 0 \end{bmatrix}$$

and the eigenvalues and eigenvectors of H are

$$\begin{array}{lll} \lambda_3 = 0 & \lambda_2 = -\frac{I_0}{\sigma_0^2}\left[\frac{\sigma_0^2-(x^2+y^2)}{\sigma_0^2}\right] & \lambda_1 = -\frac{I_0}{\sigma_0^2} \\ \vec{\mathbf{v}}_3 = (0,0,1) & \vec{\mathbf{v}}_2 = (x,y,0) & \vec{\mathbf{v}}_1 = (-y,x,0) \end{array}$$

This means that our model has the following properties:

- Inside the vessel ($x^2 + y^2 < {\sigma_0}^2$) we have two negative eigenvalues with eigenvectors in the plane orthogonal to the axis of the vessel.
- The third eigenvalue is zero and the associated eigenvector is in the direction of the axis.
- The eigenvalues λ_1 and λ_2 are maxima in absolute value when $x = y = 0$ and are equal to $-\frac{I(x=0,y=0)}{{\sigma_0}^2}$, but λ_2 decreases as a function of the distance to the center.

For the multiscale process, the model is convolved with a Gaussian kernel of standard deviation σ and the results are still valid due to the semi-group property but σ_0 has to be replaced by $\sqrt{\sigma_0^2 + \sigma^2}$.

4.2.2 Toric circular model

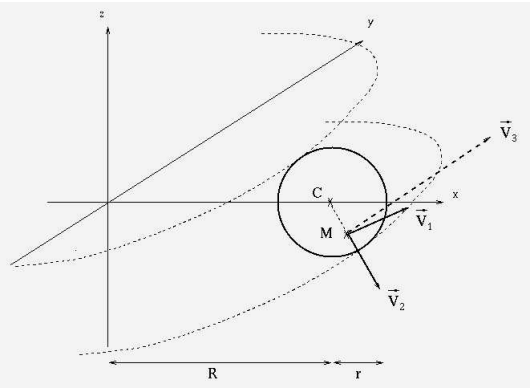

Figure 4: Toric model of a vessel.

In this case, the eigenvalues and eigenvectors are similar except that the third eigenvalue is not zero everywhere but only at the center of the vessel (see appendix A.1).

We modelize the vessel with a torus, the big circle parallel to the plane XY and with a radius R and the small circle with a radius equal to r.

The intensity function of the model is given by the expression:

$$I(x,y,z) = Ce^{-\frac{\left(R-\sqrt{x^2+y^2}\right)^2+z^2}{2\sigma_0^2}}.$$

From the circular symmetry around the (Oz) axis, we can choose $y = 0$ and $x > 0$. Then the Hessian matrix H can be expressed as:

$$H = \frac{I(x,y,z)}{\sigma_0^4} H_0$$

where

$$H_0 = \begin{bmatrix} (R-x)^2 - \sigma_0^2 & 0 & -z(R-x) \\ 0 & \frac{(R-x)\sigma_0^2}{x} & 0 \\ -z(R-x) & 0 & z^2 - \sigma_0^2 \end{bmatrix}$$

The eigenvectors and eigenvalues of H are (see Fig. 4):

$$\begin{array}{lll} \lambda_3 = -\frac{I}{\sigma_0^2}\left[\frac{x-R}{x}\right] & \lambda_2 = -\frac{I}{\sigma_0^2}\left[\frac{\sigma_0^2 - CM^2}{\sigma_0^2}\right] & \lambda_1 = -\frac{I}{\sigma_0^2} \\ \vec{\mathbf{v}}_3 = (0,1,0) & \vec{\mathbf{v}}_2 = (x-R,0,z) & \vec{\mathbf{v}}_1 = (z,0,R-x) \end{array}$$

In order to interpret the value of λ_3 depending on the curvature of the vessel $k = \frac{1}{R}$, we center the reference to the center C of the torus in the plane (Ox,Oy). With the new coordinate $x' = x - R$, we have $\lambda_3 = -\frac{I}{\sigma_0^2}\left[\frac{x'}{R+x'}\right] = -\frac{I}{\sigma_0^2}\left[\frac{kx'}{1+kx'}\right]$. When the curvature is zero, $\lambda_3 = 0$ as in the cylindrical case. Nevertheless, this result shows that a vessel curvature can lead to positive $(x > R)$ or negative $(x < R)$ values of λ_3 in the vicinity of the vessel center.

4.2.3 Cylindrical elliptical model

The elliptical section is defined by one standard deviation along the x axis, σ_x, and one standard deviation along the y axis, σ_y. The model is thus defined by:

$$I(x,y,z) = Ce^{-\frac{1}{2}\left[\left(\frac{x}{\sigma_x}\right)^2+\left(\frac{y}{\sigma_y}\right)^2\right]}.$$

The Hessian matrix can be expressed as

$$H = \frac{I(x,y,z)}{\sigma_x^2\sigma_y^2}H_0$$

where

$$H_0 = \begin{bmatrix} \sigma_y^2(X^2-1) & \sigma_x\sigma_y XY & 0 \\ \sigma_x\sigma_y XY & \sigma_x^2(Y^2-1) & 0 \\ 0 & 0 & 0 \end{bmatrix} = \begin{bmatrix} E & F & 0 \\ F & G & 0 \\ 0 & 0 & 0 \end{bmatrix}$$

with $X = \frac{x}{\sigma_x}$ and $Y = \frac{y}{\sigma_y}$.

The eigenvalues are (see appendix A.2 for more details):

$$\lambda_1 = \frac{I}{2\sigma_x^2\sigma_y^2}(E+G-\sqrt{(E+G)^2+4(F^2-EG)})$$
$$\lambda_2 = \frac{I}{2\sigma_x^2\sigma_y^2}(E+G+\sqrt{(E+G)^2+4(F^2-EG)})$$

As $F^2-EG = \sigma_x^2\sigma_y^2\left[(\frac{x}{\sigma_x})^2+(\frac{y}{\sigma_y})^2-1\right]$, we can distinguish three cases depending on the position of $M(x,y)$:

(1) $(\frac{x}{\sigma_x})^2+(\frac{y}{\sigma_y})^2-1<0$ M is *inside* the ellipse, $\lambda_1<0,\ \lambda_2<0$
(2) $(\frac{x}{\sigma_x})^2+(\frac{y}{\sigma_y})^2-1=0$ M is *on* the ellipse, $\lambda_1<0,\ \lambda_2=0$
(3) $(\frac{x}{\sigma_x})^2+(\frac{y}{\sigma_y})^2-1>0$ M is *outside* the ellipse, $\lambda_1<0,\ \lambda_2>0$

We can also study the eigenvalues along the x and y axis. In both cases, if we choose $\sigma_x > \sigma_y$, $\vec{\mathbf{v}}_1 = (0,1,0)$ and $\vec{\mathbf{v}}_2 = (1,0,0)$ and:

x axis (y = 0)	$\lambda_1 = -\frac{I}{\sigma_y^2}\left(1-\frac{y^2}{\sigma_y^2}\right)$	$\lambda_2 = -\frac{I}{\sigma_x^2}$
y axis (x = 0)	$\lambda_1 = -\frac{I}{\sigma_y^2}$	$\lambda_2 = -\frac{I}{\sigma_x^2}\left(1-\frac{x^2}{\sigma_x^2}\right)$
center (x = y = 0)	$\lambda_1 = -\frac{I}{\sigma_y^2}$	$\lambda_2 = -\frac{I}{\sigma_x^2}$

Fig. 5 shows the section of an elliptical Gaussian vessel with $\sigma_x = 5$ and $\sigma_y = 3$, and the representation of the eigenvalues $\lambda_1(x,y)$ and $\lambda_2(x,y)$.

The eigenvectors are:

$$\vec{\mathbf{v}}_i = \begin{pmatrix} \lambda_i - G \\ F \\ 0 \end{pmatrix} = \begin{pmatrix} F \\ \lambda_i - E \\ 0 \end{pmatrix} \text{ for } i \in \{1,2\}.$$

Fig. 6 shows the curves which are tangent to the eigenvectors at each point of a section of the vessel.

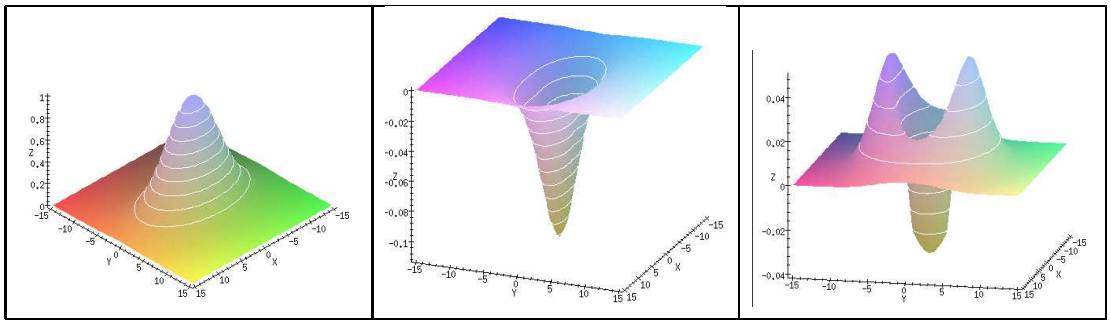

Figure 5: Left to right, surface of the Gaussian ellipse with $\sigma_x = 5$ and $\sigma_y = 3$, surface $z = \lambda_1(x, y)$, and surface $z = \lambda_2(x, y)$.

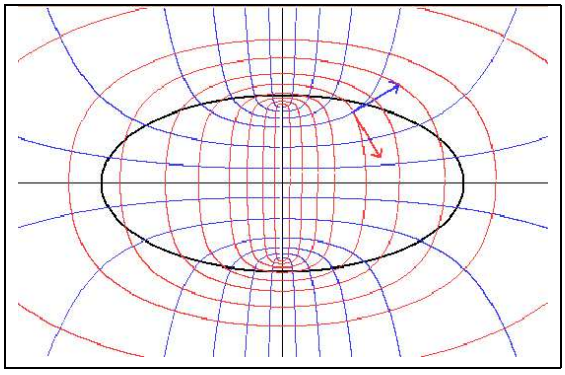

Figure 6: Representation of the curves which are tangent to the eigenvectors. In red, the curves tangent to $\vec{\mathbf{v_1}}$ and in blue the curves tangent to $\vec{\mathbf{v_2}}$.

4.2.4 Conclusion about the eigenvalues of the Hessian matrix

In the three models studied, we have at the center of the vessel one eigenvalue which is zero with the corresponding eigenvector in the direction of the axis of the vessel, and the two other eigenvalues are negative and equal if the section is circular, or approximatively equal if the section is an ellipse with $\sigma_x \approx \sigma_y$. The relations of (3) can be replaced by (5) which are more restrictive but σ_0 is unknown and the criteria remain qualitative.

$$\frac{-\lambda_1({\sigma_0}^2 + \sigma^2)}{G_\sigma * I_0} \approx 1 \text{ and } \quad \lambda_1/\lambda_2 \approx 1 \text{ and } \quad \lambda_1 \gg \lambda_3. \tag{5}$$

Furthermore, vessels sizes are usually thinner than two or three voxels and the eigenvalues are not computed at the real vessel center but at the center of a voxel. Thus, the models presented above emphasize the difficulty in relying on eigenvalues of the Hessian matrix for an accurate detection of vessel center and size. For this reason, we use eigenvalues for the discrimination of vessel-like structures and we use a gradient-based response function for the vessel extraction.

4.3 Computation of the response R_s at one scale s

A first choice for R_s can be given by equation (2) as in [KGSD95]. An advantage of this choice is to ensure that a high response means that each of the four selected points has a high gradient and the probability of being at a vessel's center is high. Nevertheless, it seems more natural to use information from the first derivative at every point of a circle than just four points. This circle $C(M, \sigma)$ is centered at the current point $M(x)$, has a radius equal to the scale $s = \sigma$, and is parallel to the eigenvectors $\vec{\mathbf{v_1}}$ and $\vec{\mathbf{v_2}}$. We experimented with three different response functions defined as the *minimum*, the *median*, and the *mean* of the first derivative in the radial direction for every point of $C(M, \sigma)$. Although the *minimum* allows a better discrimination of vessels structures, and the *median* allows a better extraction of the tangent vessels, we globally obtained better results with the *mean*, which is more robust to noise and is better at preserving the junctions and the small vessels.

In order to increase the robustness of the method, we propose instead to use the integral response:

$$R_\sigma(x) \; = \; \frac{1}{2\pi} \int_{\alpha=0}^{2\pi} -\nabla_\sigma I(x + \sigma \vec{\mathbf{v}}_\alpha).\vec{\mathbf{v}}_\alpha d\alpha \tag{6}$$

with $\vec{\mathbf{v}}_\alpha = cos(\alpha)\vec{\mathbf{v}}_1 + sin(\alpha)\vec{\mathbf{v}}_2$. This integral is computed using $N = E(2\pi\sigma + 1)$ points along the circle $C(M, \sigma)$, where $E(x)$ is the integer part of x, it leads to the discrete formulation:

$$R_\sigma(x) \; = \; \frac{1}{N} \sum_{i=0}^{N-1} -\nabla_\sigma I(x + \sigma \vec{\mathbf{v}}_\alpha).\vec{\mathbf{v}}_\alpha, \;\; \alpha = 2\pi i/N. \tag{7}$$

where $\vec{\mathbf{a}}.\vec{\mathbf{b}}$ denotes the vector product of $\vec{\mathbf{a}}$ and $\vec{\mathbf{b}}$.

4.4 Normalization

4.4.1 Standard normalization

One difficulty with multiscale approach is that we want to compare the result of a response function at different scales while the intensity and its derivatives are decreasing functions of scale. Lindeberg [Lin94, Lin96] introduced the notion of normalized derivatives in order to deal

with this problem. If the scale t is defined as $t = s^2 = \sigma^2$ where σ is the standard deviation of the Gaussian, the γ–**normalized derivative** ∂_γ is defined as

$$\frac{\partial_\gamma (I * g_t)}{\partial x} = t^{\frac{\gamma}{2}} \frac{\partial (I * g_t)}{\partial x} \tag{8}$$

where $g_t = G_{\sqrt{t}} = G_\sigma = G_s$. The value of γ is chosen to allow the response $R_t(I_0)$ to be maximal for a scale corresponding to the size of the structure we want to detect. In practice, we need a structure model in order to estimate the value of γ. We usually take an image model as a defined function $I_0(M)$, then we decide which points we want to detect (for example, the edges) and calculate their positions $P \subset \mathbb{R}^n$ in the image $I_t(M)$ at a scale t. Finally, we calculate the value of the scale $t_{max}(\gamma)$ which gives a maximum for the response function $R_t(I_0)$ at the points $M \in P$. Then we choose the value of γ that gives $t_{max}(\gamma) = s$ where s is the size of the structure. For instance, for edge detection purposes, Lindeberg [Lin96] obtained for a Gaussian blob the value $\gamma = \frac{3}{2}$. At a scale t, our model with a constant $C > 0$ leads to $L(x, y, z) = I_t(x, y, z) = I_0 * g_t = C g_{t_0+t}$. We want to detect the axis of the vessel which is defined by $x = y = 0$. The response at $M(0, 0, z)$ is:

$$R(I_0, t) = \frac{1}{2\pi\sqrt{t}} \int_{M \in C_{\sqrt{t}}} |\nabla L(x, y, t)(M).\vec{\mathbf{n}}| \, dM \tag{9}$$

which corresponds to the mean of the vector product of the gradient with the unit radial vector along the circle of center $M(0, 0, z)$ and of radius $\sqrt{t} = \sigma$. The gradient is $\nabla L(x, y, t) = \frac{-L(x,y,t)}{t+t_0}(x, y)$ and the normal vector $\vec{\mathbf{n}} = \frac{1}{\sqrt{x^2+y^2}}(x, y)$, with $x^2 + y^2 = t$, so:

$$|\nabla L(x, y, t)(M).\vec{\mathbf{n}}| = C \frac{\sqrt{t}}{2\pi \, (t + t_0)^2} \, e^{-\frac{t}{2(t+t_0)}}.$$

This last expression is no longer a function of M, then its mean along the circle is straightforward $R = \frac{C\sqrt{t}}{2\pi(t+t_0)^2} e^{-\frac{t}{2(t+t_0)}}$.

The normalized response R_N is defined by $R_N = t^{\gamma/2} R$.

The maximum normalized response at the center of a vessel is then reached for:

$$\begin{aligned} t_{max} &= h(\gamma) t_0 \quad \text{with } \gamma \in [0, 3[\\ h(\gamma) &= \frac{2\gamma - 3 + \sqrt{21 - 4\gamma}}{2(3 - \gamma)} \end{aligned} \tag{10}$$

(more details can be found in appendix A.3).

As we want $t_{max} = t_0$ (which is equivalent to $s_{max} = s_0$), γ must verify $h(\gamma) = 1$ which leads to $\gamma = \frac{5}{4}$. (Fig. 7).

4.4.2 Zoom-invariant criterion for normalization

If we take into account the fact that several vessels of various radii interact with each other, another criterion for normalization is to choose γ so that the maximum response at the center of a vessel doesn't depend on the size of this vessel. This choice will avoid privileging vessels of certain radii in the multiscale integration. For example, if the maximum response at the center of a big vessel is higher than the maximum response at the center of a small vessel, and the two vessels are neighbours, the big vessel may create side effects that would disturb the extraction of the small vessel in the multiscale integration. Moreover, finding a threshold to extract the centerlines in the final image will be more difficult.

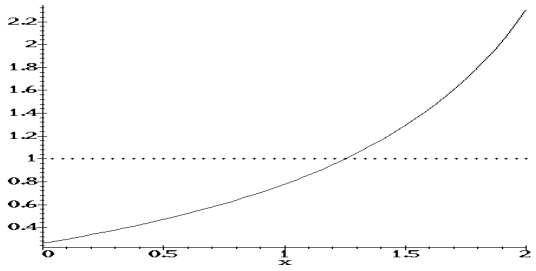

Figure 7: Representation of the function $h(\gamma)$ which shows the evolution of the scale which gives a maximum response depending on γ and t_0: $t_{max} = h(\gamma)t_0$.

This normalization requires choosing a realistic value for $C(\sigma_0)$ in the current model. If we choose the constant $C = 1$, the intensity at the center of a vessel would decrease when the radius σ_0 increases. A first approximation is that the intensity at the center of the vessel doesn't depend on its size, which leads to the constant $C = 2\pi t_0 = 2\pi\sigma_0^2$. Then, the intensity of a vessel will be equal to

$$I(x, y, z) = 2\pi t_0 g_{t_0}(x, y) = e^{-\frac{x^2+y^2}{2(t+t_0)}}.$$

As $2\pi t_0$ doesn't depend on scale or space, previous results are still valid. Maximum response is obtained for $t_{max} = h(\gamma)t_0$ and its value is:

$$\begin{aligned} R_N(t) &= 2\pi t_0 \frac{t^{\frac{\gamma+1}{2}}}{2\pi\,(t+t_0)^2}\, e^{-\frac{t}{2(t+t_0)}} \\ R_N(t_{max}) &= 2\pi t_0 \frac{t_{max}^{\frac{\gamma+1}{2}}}{2\pi\,(t_{max}+t_0)^2}\, e^{-\frac{t_{max}}{2(t_{max}+t_0)}} = 2\pi t_0 \frac{h(\gamma)^{\frac{\gamma+1}{2}} t_0^{\frac{\gamma+1}{2}}}{2\pi\,(h(\gamma)+1)^2 t_0^2}\, e^{-\frac{h(\gamma)}{2(h(\gamma)+1)}} \\ &= t_0^{\frac{\gamma+1}{2}-1} \frac{h(\gamma)^{\frac{\gamma+1}{2}}}{(h(\gamma)+1)^2}\, e^{-\frac{h(\gamma)}{2(h(\gamma)+1)}}. \end{aligned}$$

$R_N(t_{max})$ is constant for $\gamma = 1$ and we have the following relation: $t_{max} = h(1)t_0 \approx 0.78t_0$ between the size of the vessel and the scale at which it is detected. The value $\gamma = 1$ could also be deduced from the *Scaling property* defined in [Lin94] which states that γ must be equal to derivative operator order in order to have nice behaviour under spatial rescalings of original image. In practice, for each acquisition modality, a statistical study must be done to estimate the relation between the intensity at the center of a vessel and the radius of this vessel, and the response should be normalized according to this relation.

4.5 Computation of the multiscale response

The multiscale response is defined as the maximum of response set taken at different scales, see equation (1). The scales are discretized from s_l to s_h using a logarithmic scale in order to have more precision at low scales where the standard deviation is smaller and where we want to detect smaller structures. Fig. 8 shows MIPs of the normalized responses of an image. Six scales were used ranging from 1.0 to 3.5: {1.0, 1.28, 1.65, 2.12, 2.72, 3.5}. A MIP of the initial image is shown at the top left of Fig. 9, and a MIP of the multiscale response which is the maximum response across the set of scales is shown beside.

4.6 Extraction of local extrema in $R_{multi}(I_0)$

Our definition of local extrema in $R_{multi}(I_0)$ is a special case of the *Height ridge* definition [FKMP97]. Some recent work [FPE96, Lin96, Fid97] in ridge extraction use the "Marching Lines" algorithm [LC87, TG93]. In the case of vessel detection, the centerlines keep their initial position in scale-space and we propose to extract them in the multiscale response.

Why should we extract local maxima ?

For each spatial point $M(x,y,z) \in \mathbb{R}^3$, we associate the *scale-space point* $M^s(x,y,z,s) \in \mathbb{R}^3 \times \mathbb{R}_+$ where $s = s_{max}(M)$ is the scale at which the response at M is maximal (we suppose that this scale is unique which is the case for our model). We also define $\vec{\mathbf{t}}$ as a vector in the scale direction.

We define a local maximum in the scale-space response $R(M;s)$ as a point $N(x,y,z;s) \in \mathbb{R}^3 \times \mathbb{R}_+$ which is locally maximal in the directions of $\vec{\mathbf{v_1}}(M;s)$,$\vec{\mathbf{v_2}}(M;s)$ and $\vec{\mathbf{t}}$. We can easily state that for every central point M of a vessel, its associated scale-space point M^s is locally maximal in the scale-space response. If the converse is true, i.e. all the local maxima in the scale-space response are located at central points of a vessel, then detecting the centerlines is equivalent to extracting those local maxima. This assumption can be verified in the vicinity of the central points. This vicinity is obtained by pre-selection of candidates (paragraph 4.2).

The local maxima in the multiscale response.

We define the local maxima in the multiscale response R_{multi} as the points $M(x,y,z) \in \mathbb{R}^3$ that are locally maximal in the directions of $\vec{\mathbf{v_1}}(M;s)$ and $\vec{\mathbf{v_2}}(M;s)$. If M is a local maximum in the multiscale response, then its associated scale-space point M^s is also a local maximum in the scale-space response R. The reciprocal is true only if each spatial point has no more than one local maxima along scale. Making this assumption is equivalent to assuming that a point can not be at the center of several vessels of different sizes which seems realistic.

Thus, making the above assumptions, we restrict ourselves to extracting the local maxima in the multiscale response.

In practice, we use equation (11) as a characterization of the local extrema.

$$\begin{aligned} R_{multi}(M) \;&\geq\; R_{multi}(M+\vec{\mathbf{v}}) \\ \text{with } \vec{\mathbf{v}} &\in \{\pm\vec{\mathbf{v_1}}(M;s), \pm\vec{\mathbf{v_2}}(M,s)\}. \end{aligned} \tag{11}$$

A MIP of an image of the local extrema is shown at the bottom left of Fig. 9.

4.7 Skeletonization, reconstruction and visualization

It is not an easy task to visualize the local extrema image in order to improve the interpretation of the original data image. For that purpose, we propose to extract some information from the local extrema image, to superimpose it into some 3D representation of the original data image (volume or surface rendering) or to use it for a vessel network reconstruction.

Skeletonization. *First*, we binarize the local extrema image by applying a hysteresis thresholding, with manually chosen thresholds. *Second*, we thin this result to obtain a skeleton-like representation of the vessels. Thinning is achieved by deleting the simple points. These points are the ones whose removal does not change the topology of the image. More details of the skeletonization algorithm can be found in [BM94]. The resulting skeleton is composed of pieces of curves, each of them representing a piece of vessel. *Third*, the skeleton is simplified by removing small pieces of curves. For a better visualization, the remaining curves are smoothed

using an energy minimization including data attachment. The smoothing method is derived from [Del94] and doesn't modify the localization of the extremities of each line. The result obtained is an image of the vessel axes.

Reconstruction. The centerline image also contains information about the size of the vessel, which is proportional to the scale at which the current point has been extracted. The relation between a vessel size and the scale at which it was detected was given in paragraph 4.4.2. The bottom right image of Fig. 9 represents a MIP of the centerlines obtained, where central points are colored according to the scale at which they have been extracted, six colors are used ranging from blue to red for the six single-scale responses shown in Fig. 8.

Each piece of vessel is described by a sequence of points $\{c_i\}$, each of them being associated with an estimated radius r_i. We reconstruct each segment $[c_i, c_{i+1}]$ independently. If the orthogonal projection c of a point M on the line $c_i c_{i+1}$ is into the segment $[c_i, c_{i+1}]$, we estimate the radius in c, and deduce from it the intensity in M with equation (4). This way, we reconstruct a grey-level image and we visualize easily all the reconstructed vessels with an isosurface.

Visualization. The usual means of visualizing the vessel network are not effective.

On the one hand, MIPs can mislead the physicians because they don't contain information about the relative position of the vessels in depth. One can add depth-cueing to them but a high intensity vessel located behind a low intensity vessel may still appear to be in front of it, or hide it.

On the other hand, an isosurface of the initial image can account for the the *relative position* of the vessels, but it contains *partial information* about the image which is insufficient. With a low threshold an isosurface contains the small vessels but they are hidden by the big vessels. With a high threshold, it contains only the thickest vessels as shown in Fig. 2.

In both cases, MIP or isosurface, the superimposition of the detected 3D centerlines can help the interpretation of the real vessel network. Moreover, an isosurface of the reconstructed vessel network have the advantages of an initial image isosurface without having its drawbacks, because all vessels are reconstructed with the same centerline intensity. Thus, it can help to understand the real vessel network.

5 Results

We have tested our algorithm on ten images $128 \times 128 \times 128$ of varying complexity. In the studied images, small vessels have an lower intensity than bigger ones. This leads us to use a parameter γ slightly lower than 1 for the normalization. Empirically, we found that 0.75 gave good results.

The parameters s_l and s_h must be chosen according to the radius of the thinnest and the thickest vessels in the initial image. The algorithm was run with eight scales ranging from 0.5 to 4. The time used for computing the response of the extrema was 7 minutes with an AlphaStation 500, 400 MHz. Then, after manual thresholding for binarization, the skeletonization and the smoothing of the centerlines take a few seconds. The results on four different images are shown in Fig. 10, 11, 12.

The following interesting points are emphasized: most of the junction are detected without any discontinuity, tangent vessels are detected separately, some vessels with small radius and low intensity which are difficult to visualize in MIPs are well detected. A few illustrations of

these properties are designated in the images by the letters J (Junction), T (Tangency), E (Enhancement), and L (Loop).

6 Conclusion and future work

We introduced a model of 3D vessels which allows us to choose several parameters of the multiscale detection. The advantages of this model based detection is *first* to better understand the pre-selection of central points according to the Hessian matrix eigenvalues, *second* to find a good normalization, and to know the exact relation between the scale at which the response is maximal and the size of the vessel (equation (10)). The algorithm has already a good behavior and promising results, but some local problems occurring at junctions or tangent vessels have to be studied more thoroughly. Finally, we plan to use our method with other acquisition modalities such as Magnetic Resonance Angiography or CT images, and to use also the vessel information to help in the detection and the segmentation of aneurysms.

Acknowledgements
The authors want to acknowledge the contributions of Yves Trousset and Régis Vaillant from GEMSE, Buc, France. This work was funded in part by GEMSE (General Electric Medical System Europe). They also want to thank Janet Bertot for her precious corrections.

A Appendix

A.1 Eigenvalues for a toric model with circular section

If we modelize the vessel with a torus, the big circle parallel to the plane XY and with a radius R and the small circle with a radius equal to r.

The square distance from a given point $M(x,y,z)$ to the axis of the torus is given by:

$$\left(R - \sqrt{x^2+y^2}\right)^2 + z^2$$

derived from the cylindrical model, we can take the following function of intensity:

$$I(x,y,z) = Ce^{-\frac{\left(R-\sqrt{x^2+y^2}\right)^2+z^2}{2\sigma_0^2}}$$

The first and second derivatives are:

$$\begin{aligned}
\frac{\partial I}{\partial x} &= \frac{Ix}{\sigma_0^2}\left(\frac{R}{\sqrt{x^2+y^2}} - 1\right) \\
\frac{\partial^2 I}{\partial x \partial y} &= \frac{Ixy}{\sigma_0^2}\left[\frac{1}{\sigma_0^2}\left(\frac{R}{\sqrt{x^2+y^2}} - 1\right)^2 - \frac{R}{(x^2+y^2)^{\frac{3}{2}}}\right] \\
\frac{\partial^2 I}{\partial x^2} &= \frac{Ix^2}{\sigma_0^4}\left(\frac{R}{\sqrt{x^2+y^2}} - 1\right)^2 + \frac{I}{\sigma_0^2}\left[\frac{Ry^2}{(x^2+y^2)^{\frac{3}{2}}} - 1\right] \\
\frac{\partial^2 I}{\partial z^2} &= \frac{I}{\sigma_0^4}(z^2 - \sigma_0^2)
\end{aligned}$$

$$\frac{\partial^2 I}{\partial x \partial z} = -\frac{Ixz}{\sigma_0^4}\left(\frac{R}{\sqrt{x^2+y^2}} - 1\right)$$

From the circular symmetry around Oz axis we can choose $y = 0$ and $x > 0$, then the Hessian can be expressed as:

$$H = \frac{I(x,y,z)}{\sigma_0^4} H_0$$

where

$$H_0 = \begin{bmatrix} (R-x)^2 - \sigma_0^2 & 0 & -z(R-x) \\ 0 & \frac{(R-x)\sigma_0^2}{x} & 0 \\ -z(R-x) & 0 & z^2 - \sigma_0^2 \end{bmatrix}$$

The determinant of $H_0 - \lambda Id$ is:

$$\begin{aligned} det &= \left(\frac{(R-x)\sigma_0^2}{x} - \lambda\right)\left[\left((R-x)^2 - \sigma_0^2 - \lambda\right)\left(z^2 - \sigma_0^2 - \lambda\right) - z^2(R-x)^2\right] \\ &= \left(\frac{(R-x)\sigma_0^2}{x} - \lambda\right)\left[\lambda^2 - \lambda\left((R-x)^2 + z^2 - 2\sigma_0^2\right) + \sigma_0^4 - \sigma_0^2\left((R-x)^2 + z^2\right)\right] \\ &= \left[\frac{(R-x)\sigma_0^2}{x} - \lambda\right]\left[\lambda - \left((R-x)^2 + z^2 - \sigma_0^2\right)\right]\left[\lambda + \sigma_0^2\right] \end{aligned}$$

and the eigenvalues of H_0 are:

$$\begin{array}{lll} \lambda_3 = \dfrac{(R-x)\sigma_0^2}{x} & \lambda_2 = (R-x)^2 + z^2 - \sigma_0^2 & \lambda_1 = -\sigma_0^2 \\ \vec{\mathbf{v}}_3 = (0,1,0) & \vec{\mathbf{v}}_2 = (x-R,0,z) & \vec{\mathbf{v}}_1 = (z,0,R-x) \end{array}$$

and the eigenvalues of H:

$$\begin{aligned} \lambda_3 &= -\frac{I}{\sigma_0^2}\left(\frac{x-R}{x}\right) \\ \lambda_2 &= -\frac{I}{\sigma_0^2}\left[1 - \left(\frac{CM}{\sigma_0}\right)^2\right] \\ \lambda_1 &= -\frac{I}{\sigma_0^2} \end{aligned}$$

A.2 Eigenvalues for a cylindrical model with elliptical section

The elliptical section is defined by one standard deviation along the x axis: σ_x and one standard deviation along the y axis: σ_y. The model is then defined by:

$$I(x,y,z) = Ce^{-\frac{1}{2}\left[\left(\frac{x}{\sigma_x}\right)^2 + \left(\frac{y}{\sigma_y}\right)^2\right]}$$

The Hessian matrix can be expressed as

$$H = \frac{I(x,y,z)}{\sigma_x^2\sigma_y^2} H_0$$

where

$$H_0 = \begin{bmatrix} \sigma_y^2(X^2-1) & \sigma_x\sigma_y XY & 0 \\ \sigma_x\sigma_y XY & \sigma_x^2(Y^2-1) & 0 \\ 0 & 0 & 0 \end{bmatrix} = \begin{bmatrix} E & F & 0 \\ F & G & 0 \\ 0 & 0 & 0 \end{bmatrix}$$

with $X = \frac{x}{\sigma_x}$ and $Y = \frac{y}{\sigma_y}$.

The determinant of $H_0 - \lambda Id$ is

$$\begin{aligned} det &= -\lambda\left[\lambda^2 - \lambda(E+G) + EG - F^2\right] \\ &= -\lambda\left[\lambda^2 - \lambda\left(\sigma_y^2X^2 + \sigma_x^2Y^2 - \sigma_x^2 - \sigma_y^2\right) + \sigma_x^2\sigma_y^2\left(1 - X^2 - Y^2\right)\right] \end{aligned}$$

Let $P(\lambda) = \lambda^2 - \lambda(E+F) + EF - G^2$,
the determinant of P is

$$\Delta = (E+G)^2 - 4(EG - F^2) = (E-G)^2 + 4F^2 > 0 \text{ if } \sigma_x \neq \sigma_y$$

$$\lambda_1 = \frac{1}{2}(E+G-\sqrt{\Delta}) \quad ; \quad \lambda_2 = \frac{1}{2}(E+G+\sqrt{\Delta})$$

The expression of the eigenvalues is $\frac{1}{2}(E+G \pm \sqrt{(E+G)^2 + 4(F^2-EG)})$ where $F^2 - EG = \sigma_x^2\sigma_y^2\left[(\frac{x}{\sigma_x})^2 + (\frac{y}{\sigma_y})^2 - 1\right]$. We can then distinguish three cases depending on the position of $M(x,y)$:

(1)	$(\frac{x}{\sigma_x})^2 + (\frac{y}{\sigma_y})^2 - 1 < 0$	M is *inside* the ellipse,	$E<0,\ G<0,$	$\lambda_1 < 0,$	$\lambda_2 < 0$
(2)	$(\frac{x}{\sigma_x})^2 + (\frac{y}{\sigma_y})^2 - 1 = 0$	M is *on* the ellipse,	$E+G<0,$	$\lambda_1 < 0,$	$\lambda_2 = 0$
(3)	$(\frac{x}{\sigma_x})^2 + (\frac{y}{\sigma_y})^2 - 1 > 0$	M is *outside* the ellipse,	$\sqrt{\Delta} > E+G,$	$\lambda_1 < 0,$	$\lambda_2 > 0$

We can also study the eigenvalues along the x and y axis. In both cases, $F = 0$ and H_0 is diagonal so $\vec{\mathbf{v}}_1 = (1,0,0)$ and $\vec{\mathbf{v}}_2 = (0,1,0)$ and:

x axis	$\lambda_1 = -\frac{I}{\sigma_x^2}$	$\lambda_2 = -\frac{I}{\sigma_y^2}\left(1 - \frac{y^2}{\sigma_y^2}\right)$
y axis	$\lambda_1 = -\frac{I}{\sigma_x^2}\left(1 - \frac{x^2}{\sigma_x^2}\right)$	$\lambda_2 = -\frac{I}{\sigma_y^2}$

$$\vec{\mathbf{v}}_i = \begin{pmatrix} \lambda_i - G \\ F \\ 0 \end{pmatrix} = \begin{pmatrix} F \\ \lambda_i - E \\ 0 \end{pmatrix} \text{ for } i \in \{1,2\}.$$

A.3 Expression of the maximal scale depending on γ

We want to detect the axis of the vessel which is defined by $x = y = 0$. The response at a point $M(0, 0, z)$ is given by:

$$R(I_0, t) = \frac{1}{2\pi\sqrt{t}} \int_{M \in C_{\sqrt{t}}} |\nabla L(x, y, t)(M).\vec{n}|$$

which corresponds to the mean of the vector product of the gradient with the unit radial vector along the circle of center M(0,0,z) and of radius $\sqrt{t} = \sigma$. The gradient and the normal vector $\vec{n}$ have the following expressions:

$$\begin{aligned} \nabla L(x, y, t) &= L(x, y, t) \frac{-1}{t + t_0} \begin{pmatrix} x \\ y \end{pmatrix} \\ \vec{n} &= \frac{1}{\sqrt{x^2 + y^2}} \begin{pmatrix} x \\ y \end{pmatrix} \text{ with } x^2 + y^2 = t \\ &\text{then} \\ |\nabla L(x, y, t)(M).\vec{n}| &= C \frac{\sqrt{t}}{2\pi\,(t + t_0)^2}\, e^{-\frac{t}{2(t+t_0)}} \end{aligned}$$

This last expression is no longer a function of M, then the mean of this expression along the circle is straightforward.

$$R = C \frac{\sqrt{t}}{2\pi\,(t + t_0)^2}\, e^{-\frac{t}{2(t+t_0)}}$$

The normalized response R_N is defined by $R_N = Ct^{\gamma/2}R$ and its partial derivative on t is:

$$\frac{\partial R_N}{\partial t} = C \frac{t^{\frac{\gamma-1}{2}}}{4\pi\,(t + t_0)^4} e^{-\frac{t}{2(t+t_0)}} A$$

$$\text{with } A = (\gamma - 3)t^2 + (2\gamma - 3)\, t_0\, t + (1 + \gamma)t_0^2.$$

We are looking for the value of γ which gives a maximum for the function $R_N(t)$ at $t = t_0$. Thus we want $\frac{\partial R_N}{\partial t}$ to have a positive root which corresponds to a maximum.

The determinant of this second order polynomial of t (if $\gamma \neq 3$) is $t_0^2 * (21 - 4\gamma)$. If we want the function $R_N(t)$ to have a maximum for $t \in [0, +\infty[$, the determinant must be positive and we must have $0 \leq \gamma \leq \frac{21}{4}$. Moreover, if $\gamma \geq 3$, then $A > 0$ and the function $R_N(t)$ has no maximum for $t \in [0, +\infty[$, so $0 \leq \gamma < 3$. This leads to the necessary condition $\gamma < 3$.

The sign of $\frac{\partial R_N}{\partial t}$ is then the same as $A = (\gamma - 3)(t - t_1)(t - t_2)$, with $t_1 = \frac{2\gamma - 3 + \sqrt{21 - 4\gamma}}{2(3-\gamma)} t_0 > 0$ and $t_2 = \frac{2\gamma - 3 - \sqrt{21 - 4\gamma}}{2(3-\gamma)} t_0 < 0$. The maximum response is reached for $t_{max} = t_1 = h(\gamma)t_0$ with $\gamma \in [0, 3[$ and $h(\gamma) = \frac{2\gamma - 3 + \sqrt{21 - 4\gamma}}{2(3-\gamma)}$.

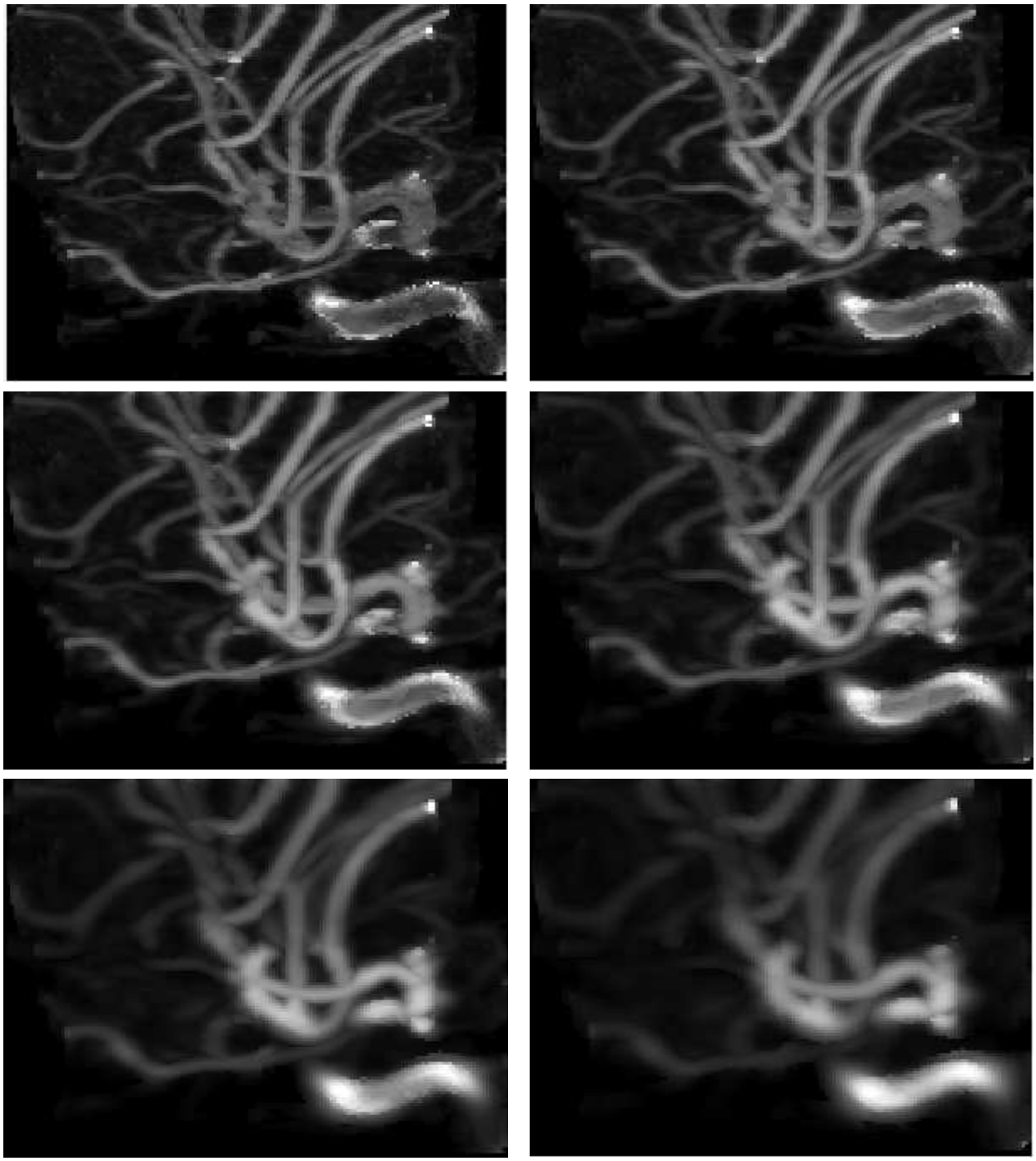

Figure 8: From left to right and top to bottom, MIPs of the responses obtained for 6 scales ranging from 1.0 to 3.5: {1.0, 1.28, 1.65, 2.12, 2.72, 3.5}.

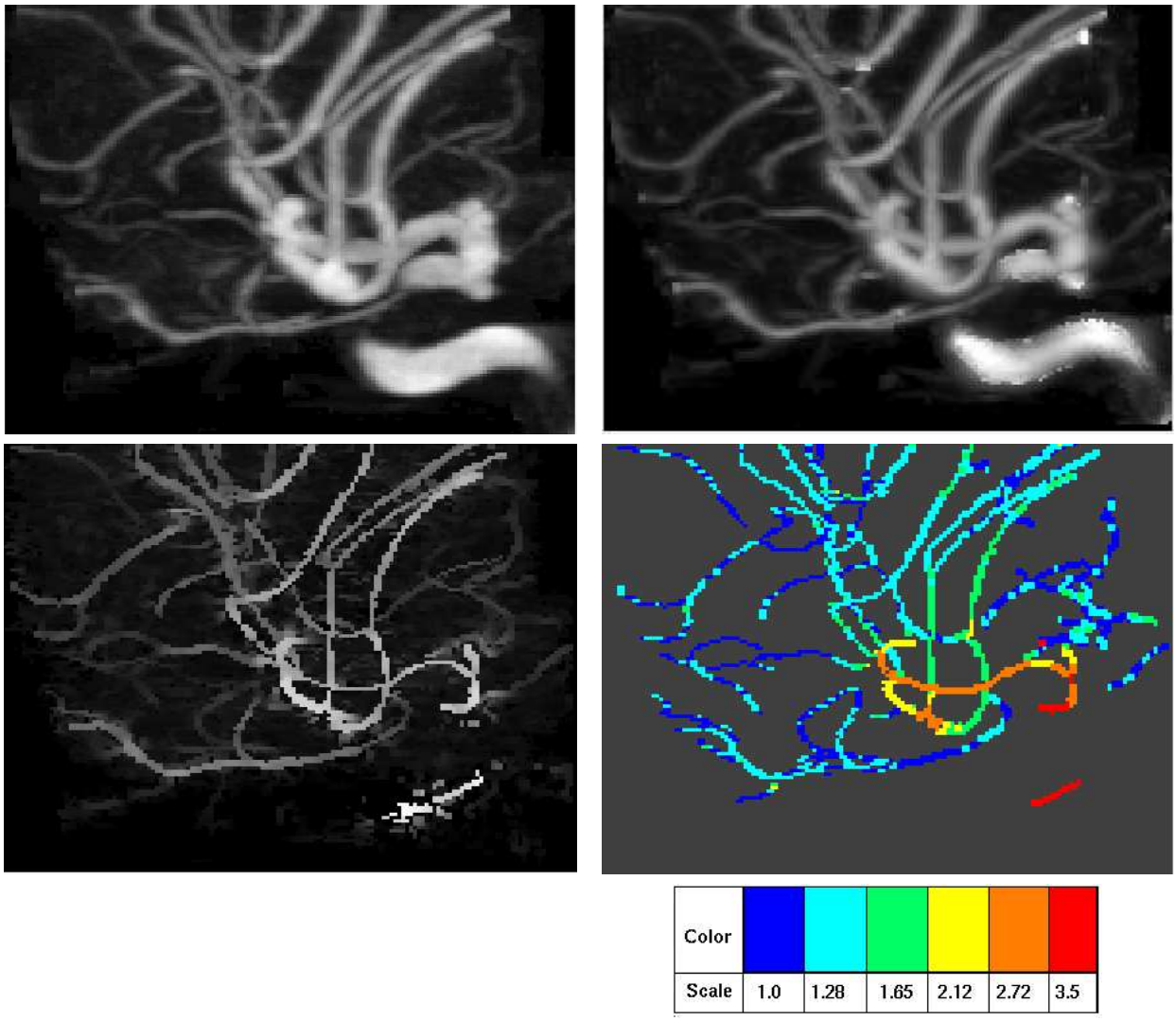

Figure 9: From left to right and top to bottom, MIPs of the initial image, the maximum response across scales, the extrema extracted from the maximum response, and the center of the vessels colored with cold colors for vessels detected at low scale and hot colors for vessels detected at high scale.

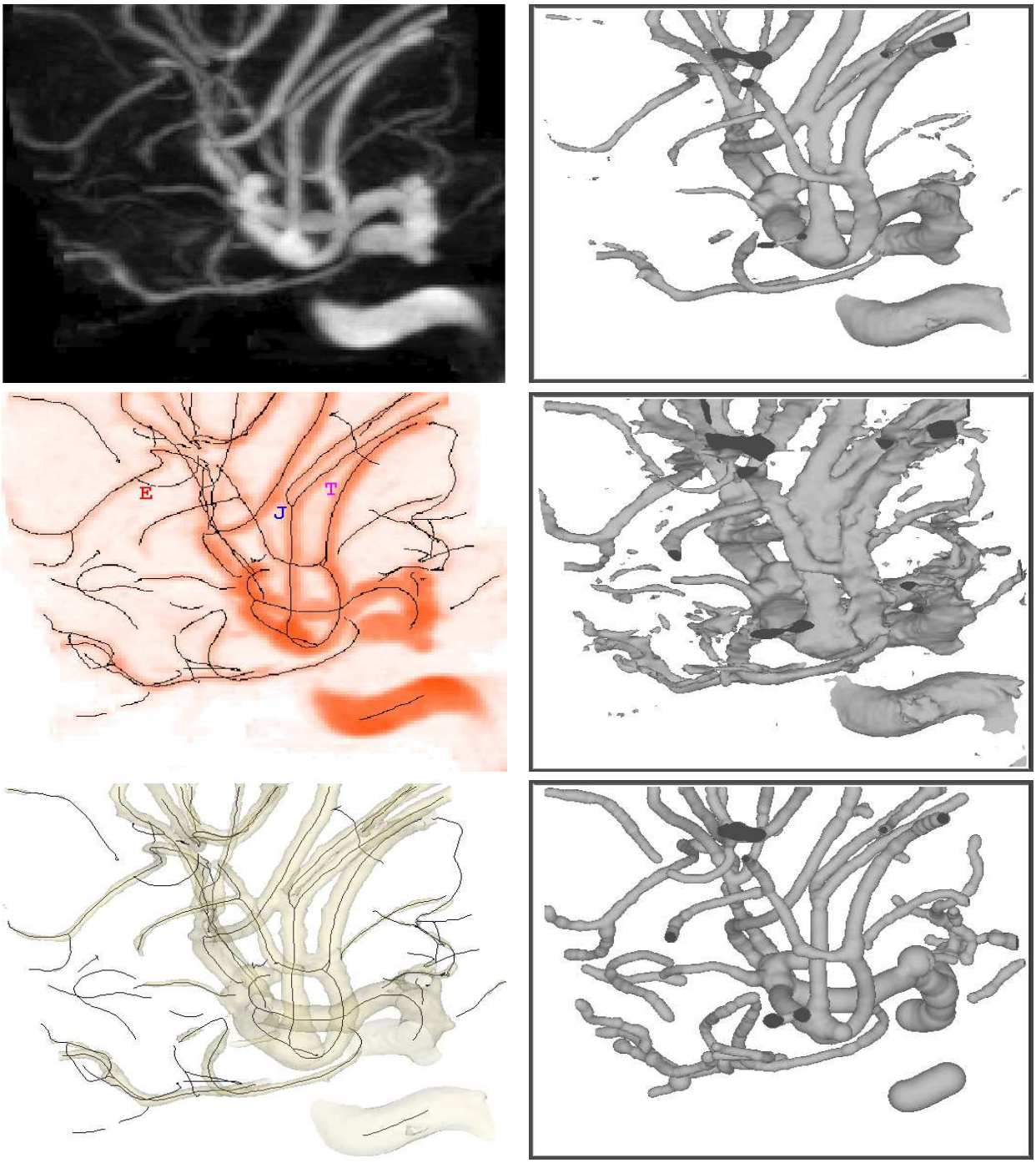

Figure 10: **Left,** top to bottom, Maximum Intensity Projection of the initial image, the detected centerlines superimposed on a Maximum Intensity Projection using a different colormap, the detected centerlines combined with an isosurface using transparency. **Right,** top to bottom, two isosurfaces of the initial image with different thresholds and an isosurface of the reconstructed image.

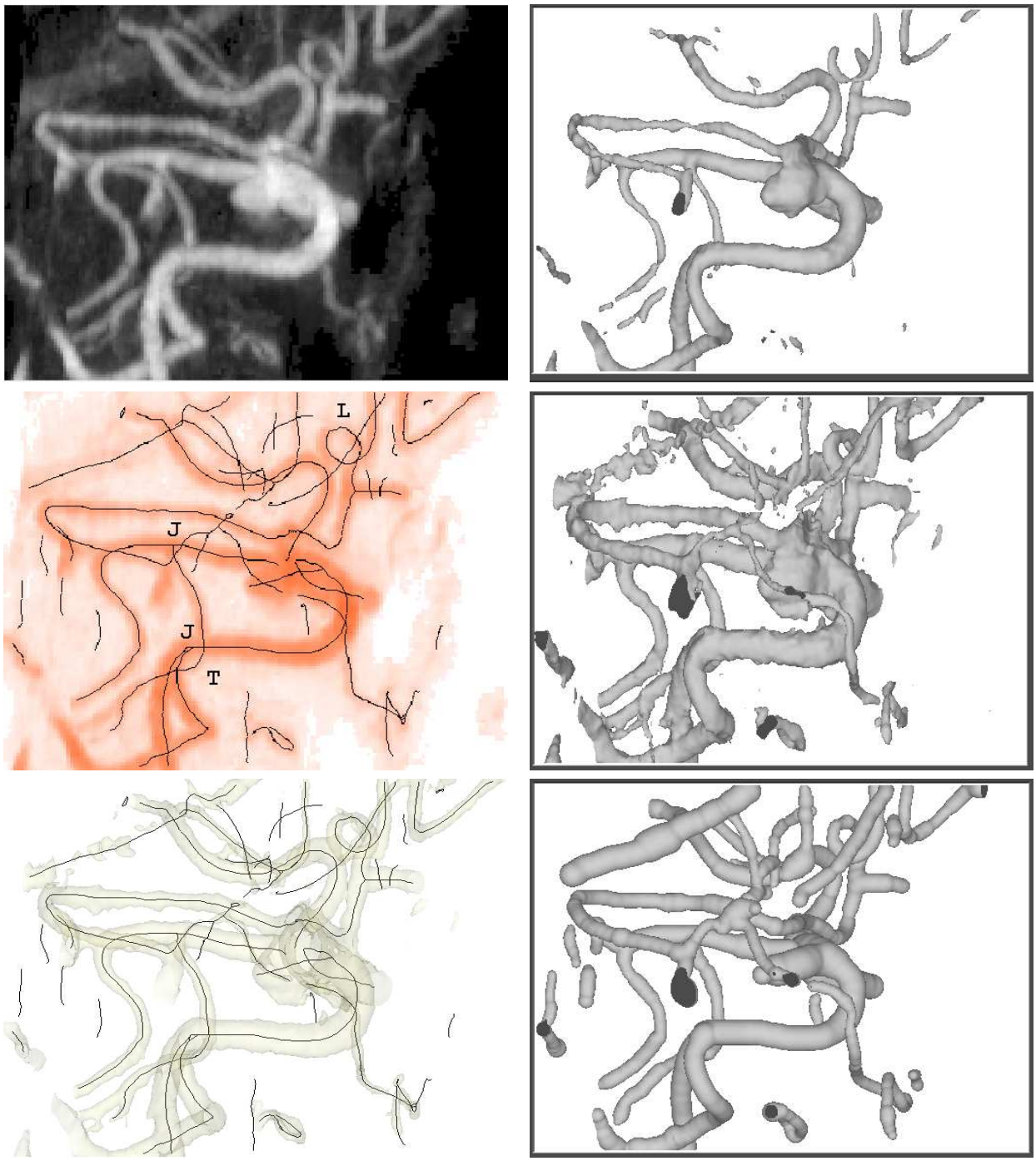

Figure 11: **Left,** top to bottom, Maximum Intensity Projection of the initial image, the detected centerlines superimposed on a Maximum Intensity Projection using a different colormap, the detected centerlines combined with an isosurface using transparency. **Right,** top to bottom, two isosurfaces of the initial image with different thresholds and an isosurface of the reconstructed image.

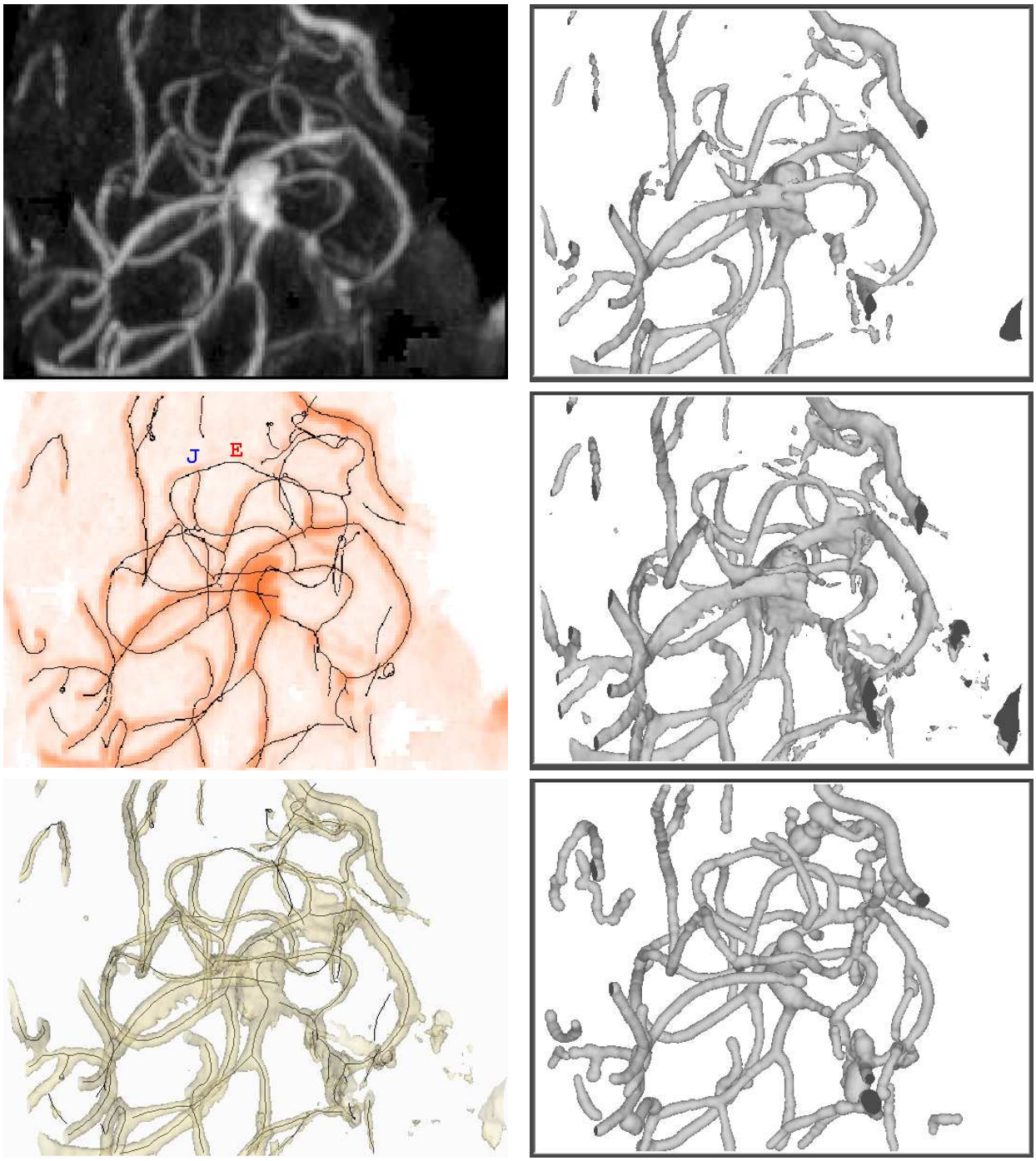

Figure 12: **Left,** top to bottom, Maximum Intensity Projection of the initial image, the detected centerlines superimposed on a Maximum Intensity Projection using a different colormap, the detected centerlines combined with an isosurface using transparency. **Right,** top to bottom, two isosurfaces of the initial image with different thresholds and an isosurface of the reconstructed image.

References

[BM94] G. Bertrand and G. Malandain. A new characterization of three-dimensional simple points. *Pattern Recognition Letters*, 15(2):169–175, February 1994.

[Can86] J. Canny. A computational approach to edge detection. *IEEE Trans on Pattern Analysis and Machine Intelligence*, PAMI-8:679–698, November 1986.

[Del94] H. Delingette. Intrinsic stabilizers of planar curves. In *3rd European Conference on Computer Vision (ECCV'94)*, Stockholm, Sweden, June 1994.

[FEPM95] D. S. Fritsch, D. Eberly, S. M. Pizer, and M. J. McAuliffe. Simulated cores and their application in medical imaging. *Information Processing in Medical Imaging*, 365–368, 1995.

[Fid97] Márta Fidrich. Following feature lines across scale. In *Scale-Space Theory in Computer Vision*, pages 140–151, Springer-Verlag, Utrecht, July 1997.

[FKMP97] J.D. Furst, R.S. Keller, J.E. Miller, and S.M. Pizer. Image loci are ridges in geometric spaces. In *First Intern Conf on Scale-Space Theory in Computer Vision*, Utrecht, July 1997.

[FPE96] J.D. Furst, S.M. Pizer, and D. Eberly. Marching cores: a method for extracting cores from 3d medical images. In *Proc. Workshop on Math. Methods in Biomed. Image Anal.*, pages 124–130, 1996.

[FPME94] D.S. Fritsch, S. M. Pizer, B. S. Morse, D.H. Eberly, and A. Liu. The multiscale medial axis and its applications in image registration. *Pattern Recognition Letters*, 15(5):445–452, 1994.

[KGSD95] T.M. Koller, G. Gerig, G. Székely, and D. Dettwiler. Multiscale detection of curvilinear structures in 2D and 3D image data. In IEEE, editor, *International Conference on Computer Vision (ICCV'95)*, pages 864–869, 1995.

[KMAV98a] K. Krissian, G Malandain, N. Ayache, R. Vaillant, and Y. Trousset. Model-based multiscale detection of 3d vessels. In *CVPR*, 1998.

[KMAV98b] K. Krissian, G Malandain, N. Ayache, R. Vaillant, and Y. Trousset. Model-based multiscale detection of 3d vessels. In *WBIA*, 1998. Extended version.

[LC87] W.E. Lorensen and H.E. Cline. Marching cubes: A high resolution 3-D surface construction algorithm. *Computer Graphics*, 21(4):163–169, 1987.

[LCBF97] C. Lorenz, I.-C. Carsen, T.M. Buzug, C. Fassnacht, and J. Weese. Multi-scale line segmentation with automatic estimation of width, contrast and tangential direction in 2d and 3d medical images. In *CVRMed-MRCAS'97*, pages 213–222, Grenoble, France, March 1997. Lecture notes in Computer Science 1205, Springer Verlag.

[Lin94] T. Lindeberg. *Scale-Space Theory in Computer Vision*. Kluwer Academic Publishers, Dordrecht, Netherlands, 1994.

[Lin96] T. Lindeberg. Edge detection and ridge detection with automatic scale selection. In *IEEE Comp. Soc. Conf. on Computer Vision and Pattern Recognition*, page 465, San Francisco, June 1996.

[Pay96] Etienne Payot. *Reconstruction Vasculaire tridimensionnelle en imagerie par rayons X.* Ph.D. dissertation, Ecole Nationale Supérieure des Télécommunication, 1996.

[PEFM98] S.M. Pizer, D. Eberly, D. Fritsch, and B.S. Morse. Zoom-invariant vision of figural shape: The mathematics of cores. *Computer Vision and Image Understanding*, 69(1):55–71, January 1998.

[SNAK97] Y. Sato, S. Nakajima, H. Atsumi, T. Koller, G. Gerig, S. Yoshida, and R. Kikinis. 3d multi-scale line filter for segmentation and visualization of curvilinear structures in medical images. In *CVRMed-MRCAS'97*, pages 213–222, March 1997. Lecture Notes in Computer Science 1205, Springer Verlag.

[TG93] J.P. Thirion and A. Gourdon. *The marching lines algorithm:New results and proofs.* Technical Report RR-1881-1, INRIA, Sophia-Antipolis, 1993.

Unité de recherche INRIA Sophia Antipolis
2004, route des Lucioles - B.P. 93 - 06902 Sophia Antipolis Cedex (France)

Unité de recherche INRIA Lorraine : Technopôle de Nancy-Brabois - Campus scientifique
615, rue du Jardin Botanique - B.P. 101 - 54602 Villers lès Nancy Cedex (France)
Unité de recherche INRIA Rennes : IRISA, Campus universitaire de Beaulieu - 35042 Rennes Cedex (France)
Unité de recherche INRIA Rhône-Alpes : 655, avenue de l'Europe - 38330 Montbonnot St Martin (France)
Unité de recherche INRIA Rocquencourt : Domaine de Voluceau - Rocquencourt - B.P. 105 - 78153 Le Chesnay Cedex (France)

Éditeur
INRIA - Domaine de Voluceau - Rocquencourt, B.P. 105 - 78153 Le Chesnay Cedex (France)
http://www.inria.fr
ISSN 0249-6399